Northumbria Research Link

Northumbria
University
NEWCASTLE

Crack Characterization in Ferromagnetic Steels by Pulsed Eddy Current Technique based on GA-BP Neural Network Model

Wang Zhenwei[a] Yuan fei[b] Pengxin Ye[b] Fasheng Qiu[c] Guiyun Tian[d] Wai Lok Woo[e]

[a] School of Aeronautics and Astronautics, University of Electronic Science and Technology of China, 611731, Chengdu, P. R. China

[b] School of Mechanical and Electrical Engineering, University of Electronic Science and Technology of China, 611731, Chengdu, P. R. China

c Key Laboratory of Nondestructive Testing (Nanchang Hang Kong University), Ministry of Education, Nanchang, 330063, P. R. China

d School of Engineering, Newcastle University, Newcastle upon Tyne, NE1 7RU, U.K

e Department of Computer and Information Sciences, Northumbria University, Newcastle upon Tyne, NE1 8ST, U.K.

Abstract: Ferromagnetic steels are widely used in engineering structures such as rail track, oil/gas pipeline and steel hanging bridge. Cracks resulted from manufacturing processes or previous loading will seriously undermine the safety of the engineering structures and even lead to catastrophic industrial accidents. Accurate and quantitative characterization the cracks in ferromagnetic steels are therefore of vital importance. In this paper, the cracks in ferromagnetic steels are detected by the pulsed eddy current (PEC) technique. Firstly, the physical mechanism of the relative magnetic permeability

of the ferromagnetic steel on the detection signal of PEC is interpreted from a microscopic level of magnetic domain wall movement. The relationship of the crack width/depth and the detection signal of PEC is then investigated and verified by numerical simulations and experimental study. Finally, the cracks are inversely characterized by using Genetic Algorithm (GA) based Back-Propagation (BP) neural network (NN) considering the nonlinearity of the crack geometric parameters with the detection signal of PEC. The prediction results indicated that the proposed algorithm can characterize the crack depth and width within the relative error of 10%. The proposed approach combining PEC and GA based BPNN has been verified to quantitatively detect cracks in ferromagnetic steel.

Key words: Ferromagnetic steels, pulsed eddy current (PEC) technique, crack, GA based BP neural network, magnetic domain wall.

1. Introduction

Ferromagnetic steels are widely used in infrastructures such as high-speed rail track, oil/gas pipeline and steel hanging bridge. The cracks are easily generated on the surface and subsurface of the ferromagnetic steels. These cracks may develop during the operating life due to the harsh working environment and cyclic loadings or as a result of flaws during manufacturing. Detection of cracks in ferromagnetic steels is critical to the safe maintenance of the infrastructure.

Presently, most of the existing techniques for the crack quantitative detection are focused on the non-magnetic materials. For instance, the conventional eddy current (EC) and pulsed eddy current (PEC) techniques are fused for detecting the locations and size

of the multiple cracks in aluminum alloys[1]; a high performance optical fiber sensor using phase-shifted fiber brag grating and balanced demodulation system was applied to evaluate the crack growth in a dog-bone 2017 aluminum plate [2].

Different from the nonmagnetic material, both the magnetic permeability as well as electric conductivity in ferromagnetic steel are important material properties parameters. Therefore, some electromagnetic nondestructive techniques such as magnetic flux leakage (MFL) [3], magnetizing-based traditional eddy current[4], alternating current field measurement (ACFM) [5], metal magnetic memory (MMM)[6] and remote field eddy current (RFEC) [7] applied for the evaluation the surface cracks in ferromagnetic metals. However, MFL is unsuitable for detecting very narrow cracks (e.g. the closed cracks) since the magnetizing-based traditional eddy current method cannot provide time-domain information of the signal. ACFM method is suitable only for linear fatigue cracks. MMM is unable to make a quantitative characterization on the shape and size of the crack, while RFEC is limited to detecting the cracks in the pipeline since RFEC phenomenon is found only in the pipeline.

Pulsed eddy current method is a new branch of the eddy current technique, which provides rich information in time-domain and frequency-domain. It has been widely applied in crack characterization in nonmagnetic materials, stress measurement, thickness measurement [8-14] and displacement monitoring [15]. Since both the magnetic permeability and electrical conductivity have influences on the magnetic flux density in PEC, PEC is appropriate technique for the crack characterization in ferromagnetic materials. To detect the subsurface crack in ferromagnetic steels,

Azizzadeh *et al.* [16] proposed a new pulsed eddy current instrument, in which a magnetizer assembly is placed below the ferromagnetic steel plate. The role of the magnetizer assembly is to magnetize the ferromagnetic steel plate into the magnetic saturation to deep the skin depth. Similarly, Rocha *et al.* [17] designed a double pulse eddy current coil, in which the two consecutive pulses of currents (up to 1500 A) is input and a high magnetic field (peak around 3.5 T) generated in the vicinity of the sample. The biased high magnetic field induces the ferromagnetic steel plate in magnetic saturation state. In magnetic saturation, the relative magnetic permeability is about 1. This feature is similar to the nonmagnetic material [4, 17-18]. However, the magnetizer either makes the structure complex or renders the system dangerous (up to 1500 A excitation current) for operators to use. Besides, the research in [19] had indicated that the different physical phenomenon would appear for the nonmagnetic material and ferromagnetic steels. Therefore, the investigation of features of the magnetic field of PEC for the ferromagnetic material is of importance to extend PEC for crack characterization in ferromagnetic steel.

The skin effect is the tendency of an alternating electric current (AC) to become distributed within a conductor (such that the current density is largest near the surface of the conductor, and decreases with greater depths in the conductor) introduces strong nonlinearity into the pulsed eddy current technique. The high magnetic permeability of ferromagnetic steel strengthens the nonlinearity greatly. Therefore, the nonlinear mapping algorithms are attracting increasing attention. A crack assessment framework for concrete structures is built using mask and region-based convolutional neural

network (Mask R-CNN) [20]. Artificial neural networks (ANNs) has been investigated for dealing with the relationship between inspection data and crack properties in nuclear steam generator tubes and their surrounding support structures [21]. The methods of support vector regression, kernelization techniques, principal component analysis, partial least squares, and methods for reducing the dimensionality of the feature space in crack recognition in magnetic flux leakage [22], pulsed eddy current NDT [23] and multi-frequency eddy current method [24].

To improve the accuracy of the quantitative cracks evaluation, the optimization algorithms such as the genetic algorithm (GA) [25], Bayesian estimation [26], particle swarm optimization algorithm [27-28], and Monte Carlo Markov chain algorithm [29] have been applied to minimize the error between the calibration and prediction values in solving the inverse problem of the electromagnetic nondestructive testing. The existing nonlinear relationship-mapping algorithms are beneficial to build the nonlinear relationship between the magnetic flux density and the crack parameters in ferromagnetic steel by PEC.

Given above, the motivations of the present work are twofold: Firstly, the proposal of an efficient approach to determine the important features of the magnetic flux density of the crack in the ferromagnetic steel by PEC. Secondly, the realization of a nonlinear relationship mapping model between the crack geometric parameters and the magnetic flux density. The paper is organized as follows: In Section 2, the numerical simulation model based on Finite element (FE) method is created. The features of the magnetic flux density are analyzed in details. The influence of the crack depth and width on the

magnetic flux density are also investigated. In Section 3, the experiment platform is presented and the simulation results are validated by experiments. Section 4 presents a GA based Back-Propagation (BP) neural network to inversely characterize the crack depth and width in ferromagnetic material. Finally, conclusions are drawn and an outline of future work is given in Section 5.

2. Numerical simulation

2.1. Principle of PEC for ferromagnetic steel

The principle of PEC technique for ferromagnetic steel is shown in Fig.1. According to the Ampere Law, as a pulse wave is excited in the spiral coil, the alternating magnetic field is produced by coils. The alternating magnetic field is defined as H_1. An eddy current would then be generated on the surface of the ferromagnetic steel specimen when the specimen is exposed to the magnetic field H_1. The eddy current would produce a magnetic field H_2 correspondingly. At the same time, when the specimen is exposed to the magnetic field H_1, the magnetic domain inside the specimen rotates along the direction of the magnetic field H_1. The specimen would be magnetized and produces a magnetic stray field H_3. It is worth pointing out that the direction of H_1 is the same as H_3, while opposite to H_2.

Therefore, when the specimen is ferromagnetic material, the magnetic field obtained by the Hall sensor is superposition of H_1, H_2 and H_3. When there are cracks in the specimen, H_2 and H_3 would be disturbed. In this case, the crack can be evaluated by analyzing the resultant magnetic field.

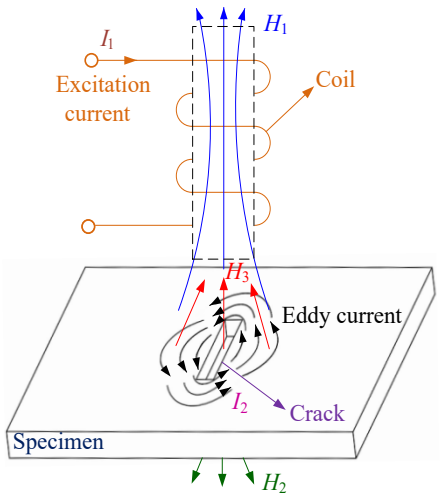

Fig.1. Principle of pulsed eddy current testing

2.2 Finite element model

The numerical simulation model consists of the air region, the detection coil and the ferromagnetic steel specimen with the crack, which is shown in Fig. 2. The geometric and electromagnetic parameters are listed in Table 1. The center point of the coil bottom surface is designed as a detection point for measuring the magnetic field signal. Since the z- component of the resultant inductive magnetic field B_z has the largest magnetic field value and contains abundant crack information, B_z is selected as the detection signal for crack evaluation.

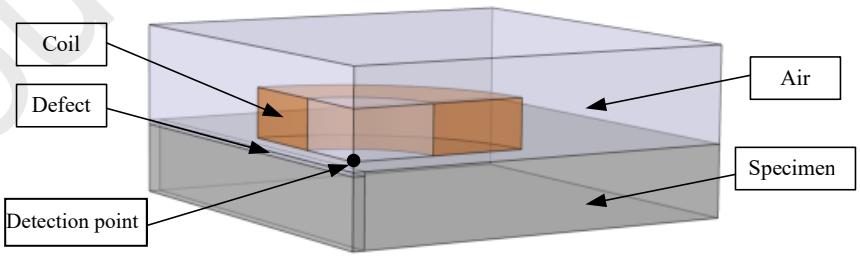

Fig.2. Simulation model

Table 1 The geometrical parameters and electromagnetic parameters of numerical model

Name	Parameters	Value	Name	Parameters	Value
Specimen (1045 steel)	Conductivity (σ/ MS•m^{-1})	7.58	Crack	Length (mm)	17.0
	Relative permeability (μ_r)	1496		Width (mm)	0.5
	Length (mm)	17.0		Height (mm)	0.3
	Width (mm)	16.5	Coil (Copper)	Conductivity (σ/ MS•m^{-1})	59.98
	Height (mm)	3.0		Relative permeability (μ_r)	1.0
Air	Conductivity (σ/ S•m^{-1})	1.0		Inter diameter (mm)	7.0
	Relative permeability(μ_r)	1.0		Outside diameter (mm)	15.0
	Length (mm)	17.0		Height (mm)	2.0
	Width (mm)	17.0		Turn number (mm)	300
	Height (mm)	4.0		Wire diameter (mm)	0.1
				Lift-off (mm)	0.4

In simulation, the excitation signal is shown in Fig. 3. It is a rising edge excitation signal with the peak value of 0.5 A and satisfies Eq.(1):

$$\begin{cases} i_0(t) = I(1-e^{-\frac{t}{\tau_0}})sign(t) \\ sign(t) = \begin{cases} 1 & (t>0) \\ 0 & (t=0) \\ -1 & (t<0) \end{cases} \end{cases} \tag{1}$$

where $\tau_0 = L/R$, $i_0(t)$ is the excitation signal, I is the peak value of the excitation signal, L and R are the inductance and resistance of the coil, respectively.

The material of the specimen is 1045 steel in ASTM (C: 0.42 % ~ 0.50%, Si: 0.17 % ~ 0.37 %, Mn: 0.50 % ~ 0.80 %, Cr ≤ 0.25 %). The crack depth is 0.3 mm, and the width is 0.5 mm.

The magnetic flux density for the model with the crack and without the crack are

denoted as B_{z1} and $B_{z2,}$ respectively. The differential signal ΔB_z can be obtained by abstracting B_{z2} from $B_{z1.}$ ΔB_z, B_{z2} and B_{z1} are indicated in Fig.4. In simulation, ΔB_z are acquired as the detection signal because the error in the actually detection (e.g. system error, hardware error) can be remove by subtracting B_{z2} from $B_{z1.}$

From Fig.4, we can find the peak value of the B_{z1} is smaller than that of B_{z2}, and ΔB_z, is sharply increased firstly and then slowly grown in time domain, which is quite different from the phenomenon when the specimen is non-ferrite metal [1-2].

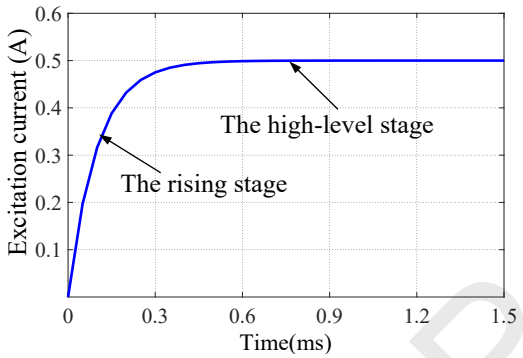

Fig.3. Excitation signal

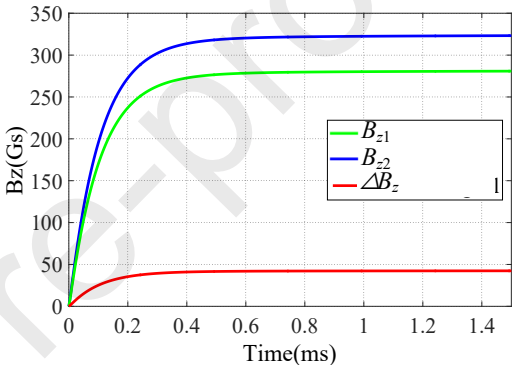

Fig.4 PEC signal for the ferromagnetic specimen

To illustrate the influences of the magnetic permeability of specimen on the resultant magnetic flux density. We consider the range of relative magnetic permeability from 1 to 10^4 order of magnitude under the room temperature condition. Therefore, we assume that the conductivity is the same as the 1045 steel of 7.58 MS/m, and the relative magnetic permeability is set as 1, 50, 100, 500 and 4000, respectively. Fig.5 shows the influence of the relative magnetic permeability of specimen on ΔB_z.

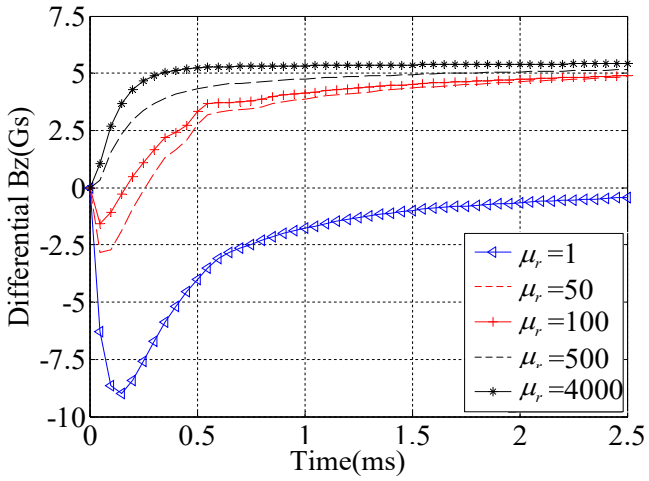

Fig.5 Influence of magnetic permeability of sample on *Bz*

For the ferromagnetic steel specimen with low relative magnetic permeability (e.g μ_r =50, 100), B_z is the equilibrium between magnetic domain wall motion-induced stray field H_3 and eddy current-induced magnetic field H_2. With zero field, the magnetic domain collect the magnetic surface flux by itself, which is plotted in Fig. 6(a). In this case, the stray field is near zero. At the rising stage (the excitation field is lower), the magnetic domain wall would be displaced with a certain distance, but the domain wall does not vanish. A weak stray field H_3 is generated as plotted in Fig. 6(b). However, it is much smaller than the current-induced magnetic field H_2, Therefore, the negative peak of ΔB_z are showing up. At the high-level stage (the excitation field is higher), the magnetic domain wall would vanish. The magnetic free pole density and corresponding stray field have increased sharply with excitation field. It is expected that $H_3 > H_2$. Hence, the ΔB_z changes qualitatively in the similar way with ferrite magnetic material with permeability of μ_r =500, 4000.

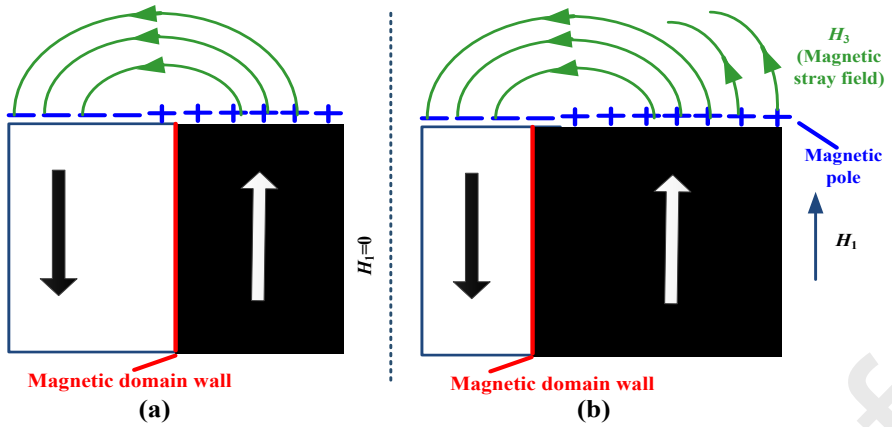

Fig. 6. A diagram of magnetic free pole due to magnetic domain wall in different magnetic field strength (a) with zero field, (b) in a mediate magnetic field strength.

For ferromagnetic steel specimen with high relative magnetic permeability (e.g. μ_r=500, 4000), the magnetic domain is saturated in low excitation field. With the movement magnetic domain wall, the magnetic free pole and corresponding stray field H_3 increase rapidly. It is expected that the time derivate of H_3 (dH_3/dt) is higher than that of the time derivate of H_2 (dH_2/dt). Accordingly, the magnetic domain wall motion-induced H_3 has the dominant influence on differential magnetic field B_z. Therefore, the negative peak value of ΔB_z vanishes.

Although the magnetic permeability varies with ferromagnetic steel specimen, the saturation density of iron-based ferromagnetic materials would the same. The density of magnetic free pole over the surface of the sample is the equal when the magnetic domain is saturated in iron-based ferrite material with different magnetic permeability. Hence, ΔB_z is the same in high magnetic excitation field.

Therefore, we can interpret the phenomenon in Fig.4 as follows: Since the relative magnetic permeability of 1045 steel is high at 1496, we observe that at the rising stage, the magnetic field at the detection point is composed of excitation magnetic field H_1,

the eddy current-induced magnetic field H_2 and the magnetic stray field H_3. The existing crack cannot change the magnetic field H_1, while H_3 is much larger than H_2 because the relative magnetic permeability of 1045 steel is high at 1496, and H_2 and H_3 are in the opposite direction, so ΔB_z at the rising edge would not appear as peak for non-ferrite specimens [9, 10, 13] by PEC. Secondly, at the high level stage, the magnetic field of the detection point is composed of the excitation magnetic field H_1 and the magnetic stray field H_3, the H_1 and the H_3 fields become smaller inthe presence of crack. Therefore, the magnetic field becomes smaller and as a result, B_{z2} becomes smaller than B_{z1}.

2.3 Relationship of the crack depth and ΔB_z

To investigate the influence of the crack depth on B_z, the crack width is set as 0.5 mm and the crack depth is set in the range of 0.1 mm to 0.8 mm with the step of 0.1 mm. Fig.7 (a) shows the relationship between ΔB_z and crack depth. When the time approaches to 1.4 ms, we acquire the value of ΔB_z and its correlation with crack depth is shown in Fig.7 (b).

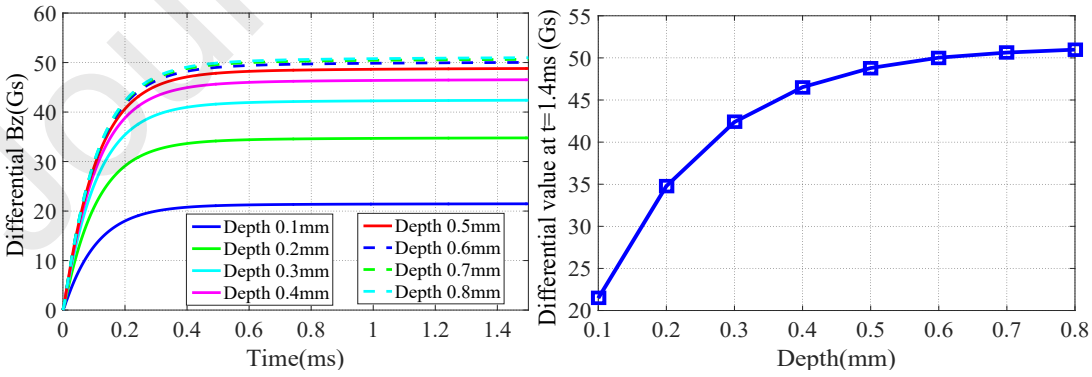

(a) (b)

Fig.7 Relationship of the crack depth and the ΔB_z (a) ΔB_z in time domain with the different crack depth, (b) tendency of the value of ΔB_z and crack depth at t=1.4ms

It is shown that the curves of ΔB_z is basically consistent for the different crack depths. With increasing crack depth, the peak value of the ΔB_z grows gradually, but the rate of increase becomes smaller. This is more obvious when the crack depth reaches 0.7 mm and 0.8 mm which is much larger than the skin depth of 0.15 mm where the difference curves are almost comparable. Therefore, for the ferromagnetic steel, the PEC is more suitable for detecting the surface crack than the subsurface one.

2.4 Relationship of the crack width and ΔB_z

To investigate the influence of the crack width, the crack depth is set as 2.0 mm, which is much deeper than the skin depth, and the width of the crack is changed from 1.0 mm to 5.0 mm with the step of 1.0 mm. The curves of ΔB_z with the different crack widths are shown in Fig. 8. The trend of the ΔB_z curves is basically consistent for different crack width. With the increase of the crack width, ΔB_z increases but the rate of growth becomes smaller when the crack width exceeds 4.0 mm.

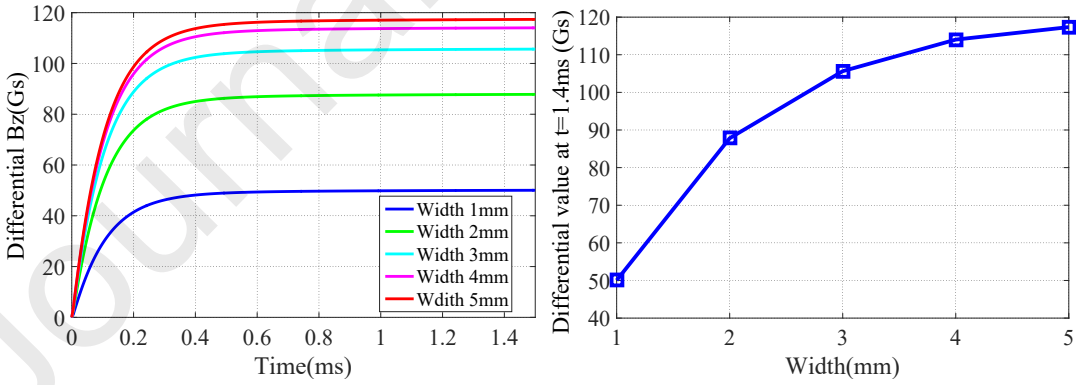

(a) (b)

Fig.8 Relationship of the crack width and the ΔB_z (a) ΔB_z in time domain with the different width, (b) tendency of the value of ΔB_z and crack width at t=1.4ms

3. Experimental verification

3.1 Experimental platform

The experimental platform consists of three main modules: signal generating, signal acquisition and signal processing system. The signal generating module includes pulse excitation signal generator, power supply, and excitation coil and Hall sensor. Signal acquisition module includes signal conditioning circuit, PCI8503 signal acquisition card and PC. Signal processing module including LabVIEW signal processing software. The specimen in this experiment is shown in Fig. 9. In Fig. 9 (a), there are 8 cracks in specimen S1, and their widths are set as 1.0 mm while the depths vary from 0.1 mm to 0.8 mm with the step increment of 0.1 mm. In Fig.9 (b), there are 5 cracks in specimen S2, and their depths are set as 2.0 mm while the widths vary from 1.0 mm to 5.0 mm with the step increment of 1.0 mm. The schematic diagram of the experiment platform and the hardware is shown in Fig.10.

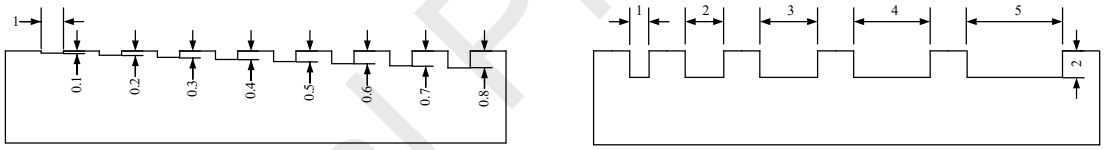

(a) (b)

Fig.9 Specimens. (a) S1: the cracks with the same width and different depths. (b) S2: the cracks with the same depth and different widths (Unit: mm)

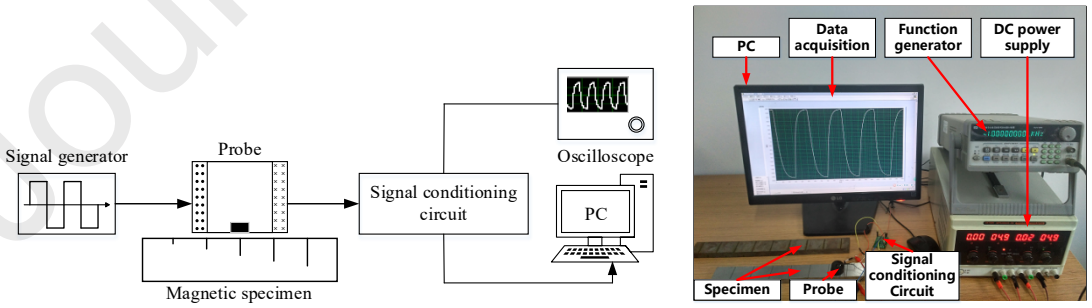

(a) (b)

Fig.10 Experimental platform (a) Schematic diagram. (b) Hardware

3.2 Experiment Verification

(1) Relationship between crack depth and detection signal

The crack width of the specimen is 1 mm, the depth is 0.1 mm ~ 0.8 mm, the step is 0.1 mm, and the output voltage of the Hall sensor is shown in Fig. 11(a). It is shown that the difference voltage is the smallest when the crack depth is 0.1 mm. The difference voltage increases gradually with the increase of the crack depth. However, the rate of increase is slow with deeper cracks. In order to quantitatively investigate the relationship between crack width and difference voltage, the difference voltages at t=0.4 ms are selected and its correlation with crack depth are shown in Fig.11 (b).

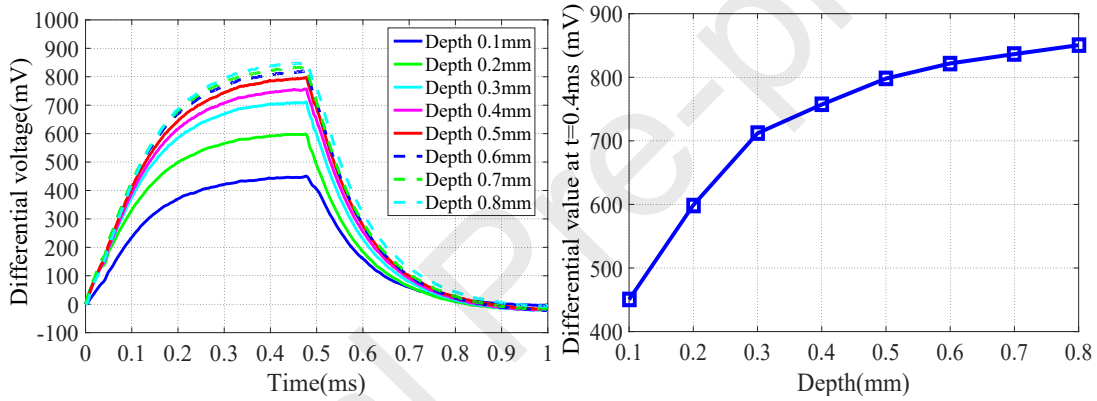

(a) (b)

Fig.11 Influence of the crack depth on detection signal. (a) Voltage signal for different crack depth, (b) Relationship between peak value and crack width (The differential value at t=0.4ms)

3.3 Relationship between crack width and detection signal

The crack depth is fixed as 1.0 mm, the width is varying in the range of 1.0 mm ~ 5.0 mm with the step of 1.0 mm, and the output signal is shown in Fig.12. It is shown that the difference signal trend of each width crack is basically consistent. When the width is 1.0 mm, the differential signal value is minimum. The difference voltage increases with the increasing width. However, when the width is 4.0 mm, the differential signal value is almost flat.

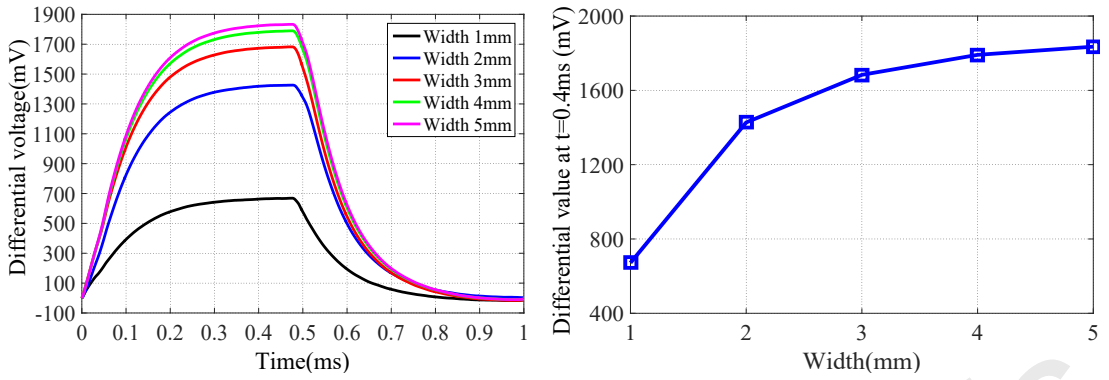

(a) (b)

Fig.12 Influence of the crack width on detection signal. (a) Voltage signal at different width, (b) Relationship of differential value and crack width at t=0.4ms

3.4 Verification of experimental results and numerical results

In simulation, B_{z1} and B_{z2} are acquired at the detection point while in experiment, the voltage V_1 and V_2 are acquired by Hall sensor after an amplifying circuit. As the Hall sensor used in this experiment is a linear sensor, the relationship between the detection voltage V in experiment and B_z in numerical simulation can be expressed as

$$\begin{cases} V_1 = kB_{z1} + b \\ V_2 = kB_{z2} + b \end{cases} \Rightarrow V = V_2 - V_1 = k(B_{z2} - B_{z1}) = kB_z \Rightarrow \frac{V}{B_z} = k \tag{2}$$

where k is a constant.

Fig.13 shows the value of k for the different crack depths and different crack widths. We can observe that when the depth is 0.1 mm or width is 1.0mm, the ratio has a large deviation from the average value when compared to the ratio for the other dimensions. The reason is that when the crack depth or width is very shallow, the influence of surface roughness on the signal is more obvious in experiment, therefore, the differences between experiment and simulation is larger. While for the other depth or width, the ratio of experiment value to the simulation value is almost kept constant and the average value of k is 16.195, therefore, it shows that the simulation result is

consistent with the experimental result.

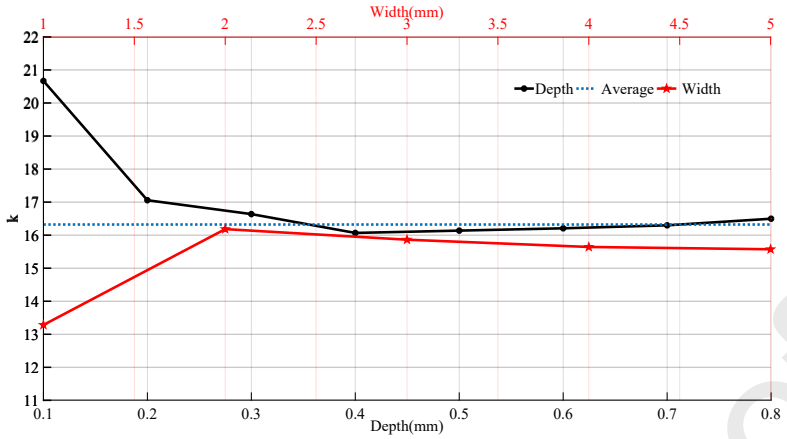

Fig 13 *k* under different crack width and depth

4. GA based BP neural network for crack characterization

4.1 GA based BP neural network

As revealed in Fig.10 (b) and Fig.11 (b), the relationship between the differential voltage and crack depth / crack width is non-linear. To address the nonlinear problem, a back-propagation (BP) neural network (NN) algorithm is considered. However, BP NN model determines its weights based on a gradient search technique, which can easily get trapped at local minima during learning as well as being sensitive to the weights initialization.

Genetic algorithm (GA) is a global optimization algorithm, being capable of finding the globally optimal solution in complex, multi-crest, non-differentiable vector spaces. Utilizing GA to search for the initial weights of the BP NN model can guarantee a relatively high probability to obtain the global optimum [30]. Therefore, a GA based BP NN is considered in this paper to overcome the shortcoming of BP neural network.

The process of optimizing BP neural network by GA includes the selection of neural network structure, the optimization of weights and the inversion of network, which is

shown in Fig.143.

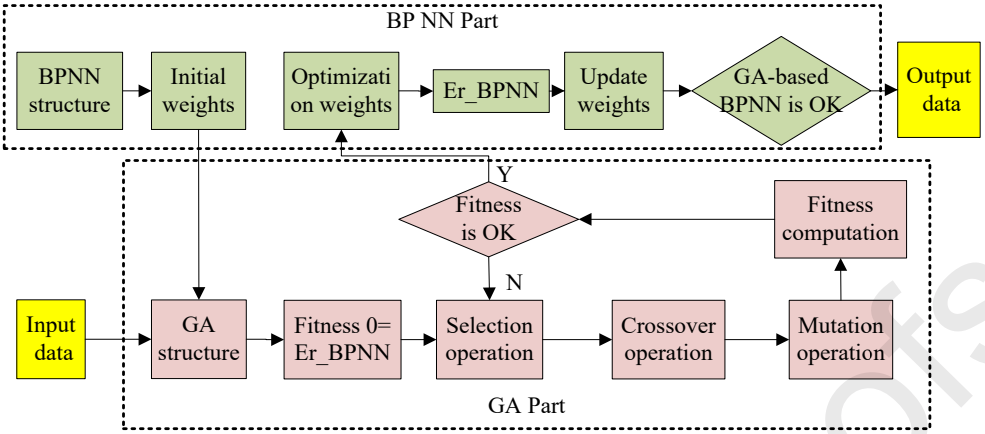

Fig.14 Flowchart of GA-based BP neural network

In optimization, the weight value is regarded as the individual in GA. The fitness value of the individual is the prediction error of the BP NN which is initialized by the individual, and then the optimal individual is produced by selection, crossover and mutation, which is the optimal weight.

4.2 Selection of training samples and validation samples

As the Hall sensor is a linear sensor, the experimental and simulation values of the same crack size are proportional. As shown in Fig.13, the proportional value k is 16.195. In order to obtain sufficient training samples, the experimental data and simulation data are designed with care. In the investigation, the experimental data are converted into the simulation data before training.

4.3 GA based BP training process

The training process of the GA based BP NN is depicted as follow.

(1) Selection of samples: The number of the training sample, validation sample and prediction sample is 140, 7, 11 for the crack depth characterization, while 80, 4, 4 for the crack width characterization. The validation samples are obtained from the

experimental study while the prediction samples are from numerical simulations. They are excluded from the training samples.

(2) The number of hidden layers: Taking into consideration the requirements on accuracy and training time, the number of hidden layers is decided to be 2.

(3) Design of the input layer and output layer: Both the input layer and output layer consist of 7 neurons. The input is the peak value of ΔB_z in time domain, and the output is the crack depth or width.

(4) The number of neurons in the hidden layer: When the number of neurons is too small the neural network does not possess enough robustness, while a too large number of neurons results in long training time and also may lead to overfitting. Therefore, the range of the number of nodes in the hidden layer is decided by [31] as 7.

$$m = \sqrt{nl} \tag{3}$$

where m is the number of neurons in the hidden layer, n is the number of neurons in the input layer and l is the number of neurons in the input layer.

(5) The initialization of interconnection weights: In our training, the interconnection weights take values from [0, 1].

Therefore, the structure of the GA based BP NN is shown in Fig.15. In which, I_i is the input neurons, H_{1i} is the neurons in the first hidden layer, H_{2i} is the neurons in the second hidden layer, and O_i is the output neurons; $w_{ij}^{[1]}$ is the weight between the i neurons in the input layer (Layer 0) and j neurons in the first hidden layer (Layer 1); $w_{ij}^{[2]}$ is the weight between the i neurons in the first hidden layer (Layer 1) and j neurons in the second hidden layer (Layer 2); and $w_{ij}^{[3]}$ is the weight between the i

neurons in the second hidden layer (Layer 2) and j neurons in the output layer (Layer 3). The activation of the j neuron in Layer l (l=1, 2, 3) is:

$$a_j^{[l]} = \sigma\left(\sum_i w_{ij}^{[l]} a_i^{[l-1]} + b_j^{[l]}\right) \tag{4}$$

where $a_j^{[l]}$ is the activation function output of the j neuron in Layer l; $a_i^{[l-1]}$ is the activation function output of the i neuron in Layer l-1; σ is the activation function; $b_j^{[l]}$ is the deviation of the j neuron in Layer l.

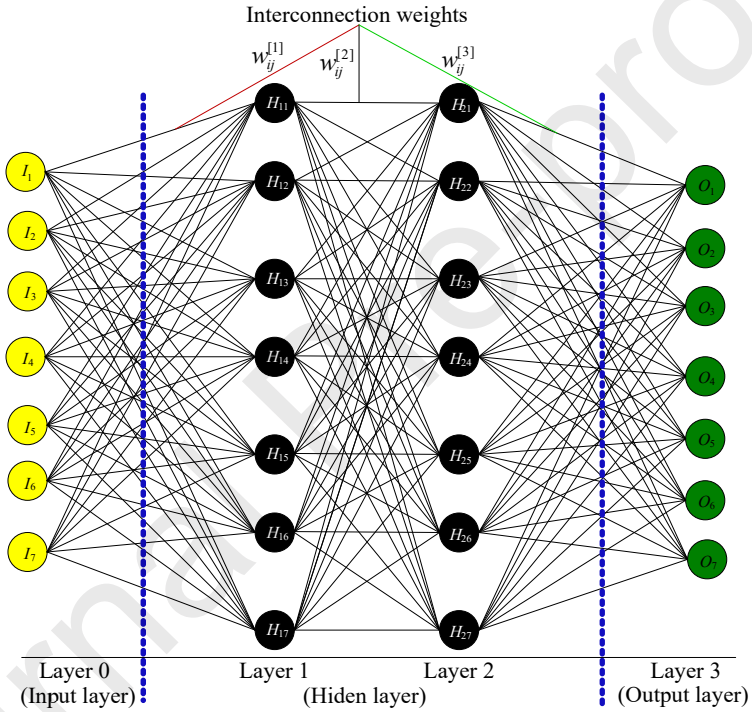

Fig.15 Structure of the GA based BP neural network (7-7-7-7)

4.4 Crack characterization and analysis

When the crossover probability and mutation probability in GA is 0.4 and 0.1, respectively, the verification and the prediction for the crack depth and crack width are shown in Fig.16. In Fig.16, '☆' denotes the verification result and '○' denotes the prediction result.

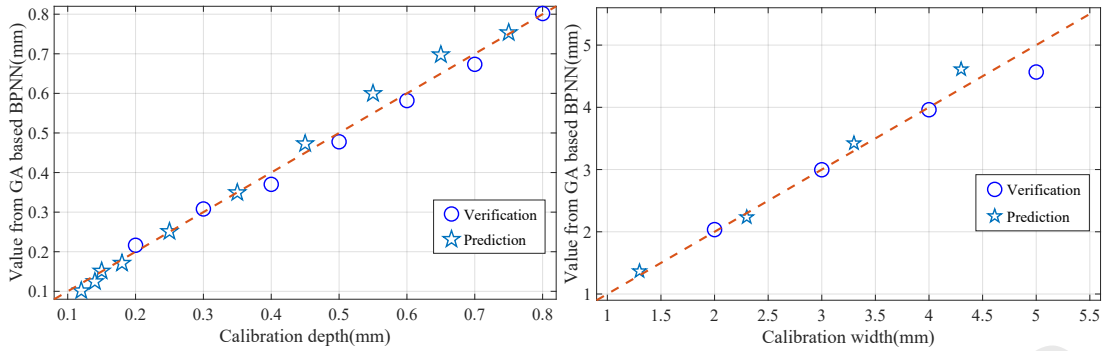

(a) (b)

Fig 16. Verification and prediction by GA based BPNN for (a) crack depth, (b) crack width

As seen in Fig.16 (a), when the experimental data are input to the GA based BPNN in Fig.15, the validation depth by BPNN based on GA is distributed around the line of the calibration depth (where the slope of the line is 1) and the discrepancy between the calibration value and the verification value verified by BPNN based on GA is within 8.15 %. The prediction value in Fig.16 (a) has shown that when the crack depth is deeper than 0.15 mm, the BPNN based on GA has successfully predicted the crack depth within the relative error of 9.0 %; however, when the crack depth is relative shallow (≤0.15mm), the inversed result has a considerable error. The reason is that when the crack depth is too shallow, the surface roughness of the specimens can introduce the serious the lift-off noise on the detection signal.

Similarly, for the crack width, Fig.16 (b) shows the error between the calibration value and the validation value from the GA based BPNN model is within 8.66 % when the crack width changes in range of 2.0 mm ~ 5.0 mm; and the prediction error is within 7.24 % when the crack width is changed in range of 1.3 mm ~ 4.3 mm.

5. Conclusion

In this paper, the differential features of the pulsed eddy current signal in time domain

for the ferromagnetic material are employed for crack characterization, which is quite different from that for the non-magnetic metals. The investigation indicated that ΔB_z for the ferromagnetic material is rapidly increasing and then converges to a constant value in time domain; while for the nonmagnetic material, ΔB_z is rapidly decreasing, arriving at the peak value and then increasing and converging to 0 in time domain. The reason result in the difference between the PEC signal of the ferromagnetic material and nonmagnetic material has been fully analyzed in terms of the magnetic domain wall movement in microstructure.

In addition, there is a strong nonlinear tendency between the magnetic flux density B_z and the crack depth/width due to the eddy current effect. To deal with the nonlinear problem, the GA based BP neural network has been proposed for crack depth and width characterization. The verification and prediction results indicated that the proposed GA based BPNN model can characterize the crack depth and width within the relative error of 10 % when the crack depth is in range from 0.15 mm to 0.8 mm while the crack width is changed in range from 1.0 mm to 5.0 mm for 1045 steel.

For the artificial cracks in the 1045 steel, the relationship between the crack geometric parameters and the PEC detection signal for the artificial cracks have been investigated and GA based BPNN is proposed to predict the crack width or depth. For the natural cracks commonly appeared in engineering, the crack width is tiny and the crack depth is the concerned crack parameters. Therefore, the crack depth characterization approach for the artificial crack can be adopted to characterize the crack depth of the natural crack.

Acknowledgements

This work is supported by the National Nature Science Foundation of China [grant number is 51675087, 61527803], the National Nature Science Foundation of Guangdong Province [grant number is 2018A030313893], and the Fundamental Research Funds for the Central Universities [grant number is ZYGX2018J067].

Reference：

[1] Wang Zhenwei, Yu, Yating, Traditional Eddy Current-Pulsed Eddy Current Fusion Diagnostic Technique for Multiple Micro-Cracks in Metals, Sensors, 2018, vol. 18, no. 9, 2909 https:/doi.org/10.3390/s18092909

[2] Wu Qi, Wang Rong, Yu, FengMing, Okabe Yoji, Application of an Optical Fiber Sensor for Nonlinear Ultrasonic Evaluation of Fatigue Crack, IEEE Sensors Journal, 2019, vol. 19, no. 13: 4992-4999, http:/doi.org/10.1109/JSEN.2019.2903323

[3] Suresh, V., Abudhahir A., Jackson Daniel, Characterization of Cracks on Ferromagnetic Tubes Using Magnetic Flux Leakage, IEEE Transactions on Magnetics, 2019, vol 55, no 5, 6200510, http:/doi.org/10.1109/TMAG.2019.2901659

[4] Deng Zhiyang, Kang Yihua, Zhang Jikai, Song Kai, Multi-source Effect in Magnetizing-based Eddy Current Testing Sensor for Surface Crack in Ferromagnetic Materials, Sensors and Actuators A:Physics, 2018, vol. 271: 24-36 https://doi.org/10.1016/j.sna.2018.01.009

[5] T. Heidari, H. Seidfaraji, S. H. H. Sadeghi, R. Moini, A Fast Analysis Technique for Electromagnetic Interaction of High-Frequency AC Current-Carrying Wires with Arbitrary-Shape Cracks in Ferrous Metals, IEEE Transactions on Magnetics, vol. 49, no. 3, pp. 1101-1107, Mar. 2013. https://doi.org/10.1109/TMAG.2012.2211106

[6] Shi Pengpeng, Jin Ke, Zhang Pengcheng, Xie Shejuan, Chen Zhenmao, Zheng Xiaojing, Quantitative Inversion of Stress and Crack in Ferromagnetic Materials Based on Metal Magnetic Memory Method, IEEE Transactions on Magnetics, vol. 54, no. 10, 2018: 6202011. https://doi.org/10.1109/TMAG.2018.2856894

[7] Luo Qingwang, Shi Yibing, Wang Zhigang, Zhang Wei, Li Yanjun, A Study of Applying Pulsed Remote Field Eddy Current in Ferromagnetic Pipes Testing, Sensors, 2017, vol 17, no 5, 1038, http:/doi.org/10.3390/s17051038

[8] Grenier M; Demers-Carpentier V; Rochette M; Pulsed eddy current: new developments for corrosion under insulation examinations, 19th World Conference on Non-Destructive Testing 2016, 13-17 June, 2016, Munich, Germany.

[9] Yu Yating, Guan Jia, Investigations of signal features of pulsed eddy current testing technique by experiments, Journal of BINDT-Insight, 2013, vol.55, no. 9: 487-492 http:/doi.org/10.1784/insi.2012.55.9.487

[10] Gui Yun Tian, Sophian, Ali. (2005). Reduction of Lift-Off Effects for Pulsed Eddy Current NDT. NDT & E International 2004, vol.38: 319-324. http:/doi.org/10.1016/j.ndteint.2004.09.007.

[11] He Yunze; Luo Feilu; Pan Mengchun, Crack Classification based on Rectangular Pulsed Eddy Current Sensor in Different Directions, Sensors and Actuators A: Physical, 2010, vol.157, no. 1, 26-31, http:/doi.org/10.1016/j.sna.2009.11.012

[12] Horan P.; Underhill P. R., Krause T. W., Pulsed Eddy Current Detection of Cracks in F/A-18 Inner Wing Spar without Wing Skin Removal using Modified Principal Component Analysis, NDT & E International, 2013, vol.55:21-27, http:/doi.org/10.1016/j.ndteint.2013.01.004

[13] Li, Yong; Tian, Gul Yun; Simm, Anthony, Fast Analytical Modelling For Pulsed Eddy Current

Evaluation, NDT & E International, 2008, vol., 41, no.6:477-483, https://doi.org/10.1016/j.ndteint.2008.02.001

[14] Park Duck-Gun, Angani, C. Sekar, Rao B. P. C., Detection of the Subsurface Cracks in a Stainless Steel Plate Using Pulsed Eddy Current, Journal of Nondestructive Evaluation, 2013,vol.32, no.4:350-353, https://doi.org/10.1007/s10921-013-0188-6

[15] Catalin Mandache, Tyrell Mcelhinney, Nezih Mrad, Aircraft Engine Blade Tip Monitoring Using Pulsed Eddy Current Technology, 4th International Symposium on NDT in Aerospace 2012 - Th.4.A.3

[16]Azizzadeh T., Safizadeh M. S. Detection of sub-surface cracks in ferromagnetic steels using a pulsed eddy current technique, Insight, 2018,vol 60, no 6,311-316, https://doi.org/ 10.1784/insi.2018.60.6.311

[17] Rocha, T. Ramos, H. G. Pasadas, D. Ribeiro, A. L.BE Ramos, HG Ribeiro, AL, Inspection of Ferromagnetic Materials Using High-Field Double Pulse Eddy Currents, International Workshop on Electromagnetic Nondestructive Evaluation (ENDE) Sep 25-28, 2016, Lisbon, Portugal, 2017,vol 42, 32-39, https://doi.org/10.3233/978-1-61499-767-2-32

[18]Wen, Dongdong, Fan, Mengbao, Cao, Binghua, Ye, Bo, Tian, Guiyun, Extraction of LOI Features From Spectral Pulsed Eddy Current Signals for Evaluation of Ferromagnetic Samples, IEEE Sensors Journal, 2019, vol 19, no 1, 189-195, https://doi.org/10.1109/JSEN.2018.2876199

[19] Qiu F, Klug M J, Tian G, et al. Influence of magnetic domain wall orientation on Barkhausen noise and magneto-mechanical behavior in electrical steel[J]. Journal of Physics D: Applied Physics, 2019, 52(26): 265001.

[20] Kim, Byunghyun, Cho, Soojin, Image-based concrete crack assessment using mask and region-

based convolutional neural network, Structural Control & Health Monitoring, 2019, vol 26, no 8, e2381, https://doi.org/10.1002/stc.2381

[21] Buck, Jeremy A. Underhill, Peter Ross Morelli, Jordan E. Krause, Thomas W.I Simultaneous Multiparameter Measurement in Pulsed Eddy Current Steam Generator Data Using Artificial Neural Networks, IEEE Transactions on Instrumentation and Measurement, 2016, vol.65, no.3:72-679, https://doi.org/10.1109/TIM.2016.2514778

[22] A. Khodayari-Rostamabad, J. P. Reilly, N. K. Nikolova, J. R. Hare, and S. Pasha, Machine learning techniques for the analysis of magnetic flux leakage images in pipeline inspection, IEEE Transactions on. Magnetics, 2009, vol. 45, no. 8: 3073-3084, https://doi.org/10.1109/ TMAG.2009.2020160

[23]A Sophian, GY Tian, D Taylor, J Rudlin, A feature extraction technique based on principal component analysis for pulsed eddy current NDT, NDT & e International 36 (1), 37-41, 2003 https://doi.org/10.1016/S0963-8695(02)00069-5

[24]T Chady, M Enokizono, R Sikora, T Todaka, Y Tsuchida, Natural crack recognition using inverse neural model and multi-frequency eddy current method, IEEE transactions on Magnetics 37 (4), 2797-2799, 2001 https://doi.org/10.1109/20.951310

[25] Hari K. C., Nabi M., Kulkarni S. V., Improved FEM Model for Crack-shape Construction from MFL Signal by using Genetic Algorithm, IET Sci., Meas. Technol., Vol. 1, no. 4: 196-200, 2007. https://doi.org/10.1049/iet-smt:20060069

[26] Khan T., Ramuhalli P., A Recursive Bayesian Estimation Method For Solving Electromagnetic Nondestructive Evaluation Inverse Problems, IEEE Transactions on Magnetics, 2008, vol. 44, no. 7:1845-1855, https://doi.org/10.1109/TMAG.2008.921842

[27] Zhang Y., Ye Z., Wang C., A Fast Method For Rectangular Crack Sizes Reconstruction In Magnetic Flux Leakage Testing, NDT & E International, 2009, vol. 42, no. 5: 369-375. https://doi.org/10.1016/j.ndteint.2009.01.006

[28] W. Han, J. Xu, P. Wang, G. Tian, Crack Profile Estimation from Magnetic Flux Leakage Signal via Efficient Managing Particle Swarm Optimization, Sensors, 2014, vol. 14, no. 6: 10361-10380. https://doi.org/10.3390/s140610361

[29] Cai C., Rodet T., Lambert M., Influence Of Partially Known Parameter on Flaw Characterization in Eddy Current Testing by using A Random Walk Mcmc Method Based On Metamodeling, J. Phys., Conf. Ser. , 2014, vol. 542, no. 1, 012009. https://doi.org/10.1088/1742-6596/542/1/012009

[30] Maofu Liu, Weili Guan, Jie Yan, Huijun Hu, Correlation identification in multimodal weibo via back propagation neural network with genetic algorithm, J. Vis. Commun. Image R. vol.60,pp.312-318,2019

[31] Z.Y.A. Ang, W.L. Woo, E. Mesbahi, Artificial Neural Network Based Prediction of Energy Generation from Thermoelectric Generator with Environmental Parameters, Journal of Clean Energy Technologies, vol. 5, no. 6, pp. 458-463, 2017. https://doi.org/ /10.1109/ICGEA.2017.7925459

Author	Contribution statement
Wang Zhenwei	Conceptualization&Investigation
Yuan Fei	Formal analysis
Pengxin Ye	Formal analysis
Fasheng Qiu	Validation
Guiyun Tian	Validation
Wai Lok Woo	Validation

Highlights

- The PEC signal for the crack in ferromagnetic material is investigated.
- The PEC signal for ferromagnetic material and for nonmagnetic material are different.
- The effect of magnetic permeability on PEC signal is interpreted in terms of the microstructure.
- A GA based BPNN model is proposed to evaluate the crack in ferromagnetic material.
- The GA based BPNN model can solve the nonlinear problem in PEC well.